

# Supervoids in the WISE-2MASS catalogue imprinting Cold Spots in the Cosmic Microwave Background

F. Finelli<sup>1,2</sup>, J. García-Bellido<sup>3\*</sup>, A. Kovács<sup>4</sup>, F. Paci<sup>5</sup>, I. Szapudi<sup>6</sup>

<sup>1</sup> *INAF-IASF Bologna, Istituto di Astrofisica Spaziale e Fisica Cosmica di Bologna*

*Istituto Nazionale di Astrofisica, via Gobetti 101, I-40129 Bologna, Italy*

<sup>2</sup> *INFN, Sezione di Bologna, Via Irmerio 46, I-40126 Bologna, Italy*

<sup>3</sup> *Instituto de Física Teórica IFT-UAM/CSIC, Universidad Autónoma de Madrid, Cantoblanco 28049 Madrid, Spain*

<sup>4</sup> *Institut de Física d'Altes Energies, Universitat Autònoma de Barcelona, E-08193 Bellaterra (Barcelona), Spain*

<sup>5</sup> *SISSA, Astrophysics Sector, Via Bonomea 265, 34136, Trieste, Italy*

<sup>6</sup> *Institute for Astronomy, University of Hawaii, 2680 Woodlawn Drive, Honolulu, HI, 96822, USA*

9 September 2018

## ABSTRACT

The Cold Spot (CS) is a clear feature in the Cosmic Microwave Background (CMB); it could be of primordial origin, or caused by a intervening structure along the line of sight. We identified a large projected underdensity in the recently constructed WISE-2MASS all-sky infrared galaxy catalogue aligned with the Cold Spot direction at  $(l, b) \approx (209^\circ, -57^\circ)$ . It has an angular size of tens of degrees, and shows a  $\sim 20\%$  galaxy underdensity in the center. Moreover, we find another large underdensity in the projected WISE-2MASS galaxy map at  $(l, b) \approx (101^\circ, 46^\circ)$  (hereafter Draco Supervoid), also aligned with a CMB decrement, although less significant than that of the CS direction. Motivated by these findings, we develop spherically symmetric Lemaitre-Tolman-Bondi (LTB) compensated void models to explain the observed CMB decrements with these two underdensities, or “supervoids”. Within our perturbative treatment of the LTB voids, we find that the Integrated Sachs-Wolfe and Riess-Sciama effects due to the Draco Supervoid can account for the CMB decrement observed in the same direction. On the contrary, the extremely deep CMB decrement in the CS direction is more difficult to explain by the presence of the CS supervoid only. Nevertheless, the probability of a random alignment between the CS and the corresponding supervoid is disfavored, and thus its contribution as a secondary anisotropy cannot be neglected. We comment on how the approximations used in this paper, in particular the assumption of spherical symmetry, could change quantitatively our conclusions and might provide a better explanation for the CMB CS.

**Key words:** cosmic microwave background - large scale structure - inhomogeneous models

## 1 INTRODUCTION

The temperature anisotropies of the Cosmic Microwave Background (CMB) provide the earliest image of the primordial density fluctuations generated during inflation. They evolve into the present distribution of Dark Matter traced by galaxies, possibly in a biased fashion. The cosmological information encoded in the spatial distribution of galaxies is revealed by several present and future programs mapping the Universe in wide area surveys, such as Pan-STARRS (Kaiser et al. 2010), DES<sup>1</sup>, DESI (Levy et al.

2013), LSST (LSST Science Collaboration et al. 2009) and Euclid (Laureijs et al. 2011; Amendola et al. 2013).

While a homogeneous and flat Universe with a cosmological constant and dark matter - the  $\Lambda$ CDM model - agrees with most of the observations, several “anomalies” remain puzzling on large angular scales in the CMB maps. Among these, a cold area in the direction  $(l, b) = (209^\circ, -57^\circ)$ , initially found as of approximately  $5^\circ$  radius in the Wilkinson Microwave Anisotropy Probe (WMAP) temperature map by Vielva et al. (2004), has been characterized in the PLANCK 2013 temperature maps with great accuracy (Ade et al. 2013). The occurrence of a decrement in the CMB temperature pattern with similar size in Gaussian simulations has been evaluated to be below 1% (Cruz et al. 2005). Although the statistical significance of the CS as an anomaly in the

\* E-mail: [juan.garciabellido@uam.es](mailto:juan.garciabellido@uam.es)

<sup>1</sup> <http://www.darkenergysurvey.org/>

CMB pattern within the  $\Lambda$ CDM cosmology can be debated, it is important to pursue physical explanations beyond assuming it is astatistical fluke.

The CS in the CMB pattern could have been originated by a primordial fluctuation on the last scattering surface or by an intervening phenomenon along the line of sight. Contamination from our galaxy or by the Sunyaev-Zeldovich effect from a cluster are quite unlikely (Cruz et al. 2006). If it were a primordial feature on the last scattering surface, the CS could be a signature of a non-perturbative effect during inflation (García-Bellido and Haugboelle 2008; Afshordi, Slosar and Wang 2011), or it might open a new exciting window onto the early Universe if caused by a cosmic texture generated during a phase transition at  $10^{16}$  GeV (Cruz et al. 2007). Alternatively, the CS could be imprinted by an intervening supervoid along the line of sight (Inoue and Silk 2006, 2007; Inoue, Sakai and Tomita 2010; Inoue 2012). While voids fill approximately 30 % of the Universe at  $z < 1$  (Colberg et al. 2005) a quantitative explanation seems to require a supervoid with radius  $\gtrsim 200 \text{ Mpc}^{-1}$ , a quite rare structure in a  $\Lambda$ CDM cosmology. Future data from CMB lensing (Das and Spergel 2008) and from 21-cm observations (Kovetz and Kamionkowski 2013) may help to further discriminate between the texture and the void hypotheses.

The supervoid hypothesis can be tested in galaxy surveys, and several investigations have been already carried out. An underdensity in the direction of the CMB cold spot has been claimed in NVSS (Rudnick et al. 2007), but its statistical significance has been debated (Smith and Huterer 2010). Granett, Szapudi and Neyrinck (2010b) imaged the cold spot region by the Canada-France-Hawaii Telescope (CFHT) ruling out the existence of a 100 Mpc supervoid with underdensity  $\delta \simeq -0.3$  at  $0.5 < z < 0.9$ . Bremer et al. (2010) reached similar conclusions from a redshift survey using the VIMOS spectrograph on the VLT. In the relatively shallow 2MASS galaxy catalogue, Francis & Peacock (2010b) found an under-density in the galaxy field in the Cold Spot region. The structure they identified induces a  $\Delta T = -7 \mu\text{K}$  depression in the CMB temperatures in the  $\Lambda$ CDM cosmology, that is not a satisfactory explanation for the CS anomaly.

In this paper and in Szapudi et al. (2015) a supervoid is indeed found in the direction of the CMB CS at a redshift compatible with previous constraints (Bremer et al. 2010; Granett, Szapudi and Neyrinck 2010b). In this paper we characterize the underdensity with the use of the recent galaxy catalogue WISE-2MASS (Kovács and Szapudi 2014) produced by joining the Wide-Field Infrared Survey Explorer (WISE, Wright et al. (2010)) with the 2-Micron All-Sky Survey (2MASS, Skrutskie et al. (2006)), whose median redshift is  $z \sim 0.14$ . (See Kovács et al. (2013) for the previous generation of catalogue based on WISE alone.) In Szapudi et al. (2015) a joint WISE-2MASS-Pan-STARRS1 catalog constructed within a  $50^\circ \times 50^\circ$  area centred on the CMB CS with photometric redshifts is used to best characterize the supervoid and determine also its deepest region at  $z \sim 0.15 - 0.25$ .

Motivated by this detection of a supervoid in the direction of the CMB CS we use a Lemaitre-Tolman-Bondi model to jointly explain the underdensity in the WISE-2MASS galaxy survey and the decrement in the CMB temperature maps. Since a correspondence between supervoids

and cold regions in the CMB temperature pattern could not be unique to the CS direction, we search for other large underdensities in the WISE-2MASS catalogue, extending Szapudi et al. (2015) who surveyed only the CS area. We find *another* underdensity located in the Northern Galactic hemisphere in the direction at ( $l \approx 101^\circ, b \approx 46^\circ$ ) with an angular size similar to the one found in the direction of the CMB CS. While this projected underdensity is even deeper than the one found in the CS region, the shallow 2MASS galaxy density maps of  $z_{mean} = 0.07$  by Rassat et al. (2013) show a large underdensity in a similar location, therefore it may be closer to us and smaller in physical size. Hereafter we refer to this underdensity as Draco Supervoid. Since this underdensity is aligned with a moderate CMB temperature decrement as well, we apply our LTB model to jointly explain the galaxy and CMB pattern in this direction.

The paper is organized as follows. In section 2 we briefly describe the PLANCK nominal mission and WMAP 9-year temperature data which we use for our analysis, and also describe the WISE-2MASS data and the two largest underdensities found. In section 3, we describe our basic LTB model for voids and the corresponding predictions for CMB temperature anisotropies, and apply our basic LTB model to the underdensities found in the WISE-2MASS catalogue. We draw our conclusions in section 4.

## 2 DATA SETS

### 2.1 CMB temperature maps

As CMB temperature maps we consider WMAP 9-year and PLANCK data. To minimize astrophysical contamination we use CMB foreground cleaned maps. For WMAP, we use the 9th year Internal Linear Combination (ILC) map at the HEALPIX (Gorski et al. 2005) resolution  $N_{\text{side}} = 1024$  publicly provided at <http://lambda.gsfc.nasa.gov/>. For PLANCK data different CMB foreground cleaned maps are provided Ade et al. (2013), and we choose the Spectral Matching Independent Component Analysis (SMICA) (Cardoso et al. 2008) map at the HEALPIX (Gorski et al. 2005) resolution  $N_{\text{side}} = 2048$ , publicly provided at <http://pla.esac.esa.int/pla/aio/planckProducts.html>.

### 2.2 WISE-2MASS galaxies

Kovács and Szapudi (2014) combined photometric information of the WISE and 2MASS infrared all-sky surveys to produce a clean galaxy sample for large-scale structure research. They apply Support Vector Machines (SVM) to classify objects using the multicolor WISE-2MASS database. They calibrate their star-galaxy separator algorithm using Sloan Digital Sky Survey (SDSS, Abazajian et al. 2009) classification, and use the Galaxy and Mass Assembly (GAMA, Driver et al. 2011) spectroscopic survey for determining the redshift distribution of the WISE-2MASS galaxy sample.

Furthermore, Kovács and Szapudi (2014) pointed out that  $W1_{\text{WISE}} - J_{2\text{MASS}} \leq -1.7$  with a flux limit of  $W1_{\text{WISE}} \leq 15.2$  mag is a simple and effective star-galaxy separator, capable of producing results comparable to the multi-dimensional SVM classification. As a further refinement, another flux limit of  $J_{2\text{MASS}} \leq 16.5$  mag is applied to have a

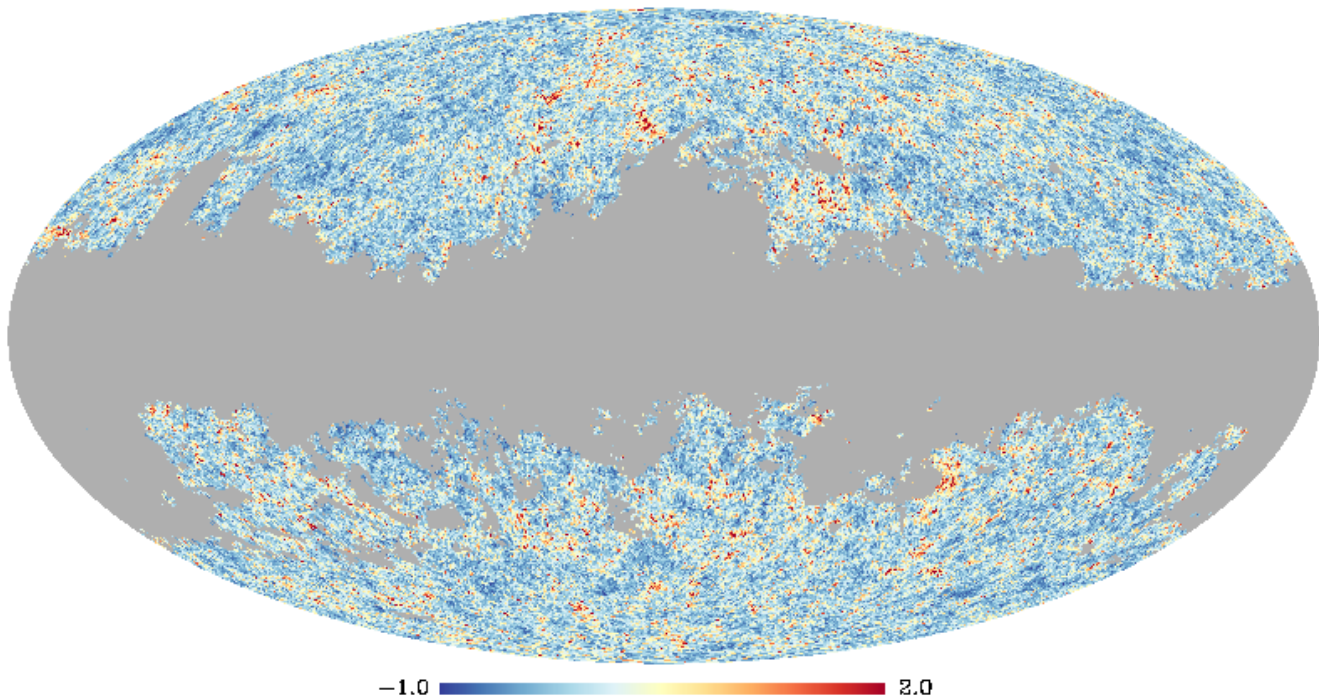


**Figure 1.** WISE-2MASS galaxy density map with the corresponding mask. See text for details.

fairly uniform all-sky dataset that is deeper than 2MASS XSC (Jarrett et al. 2000) and cleaner than WISE. The final catalogue has an estimated  $\sim 2\%$  stellar contamination among 2.4 million galaxies with  $z_{med} \approx 0.14$ .

We construct a mask to exclude potentially contaminated regions near the Galactic plane using the dust emission map of Schlegel et al. (1998). We mask out all pixels with  $E(B - V) \geq 0.1$ , and regions at galactic latitudes  $|b| < 20^\circ$ , leaving  $21,200 \text{ deg}^2$  for our purposes. The resulting galaxy density map with the corresponding mask is shown in Fig. 1.

### 2.2.1 Cold Spot region in WISE-2MASS

We first study the CMB Cold Spot region on the sky as traced by WISE-2MASS galaxies in the  $\sim 30'$  resolution 2D projection - HEALPix (Gorski et al. 2005)  $N_{side} = 128$ , therefore perform a complementary analysis to that of Szapudi et al. (2015) who measured galaxy densities in the line-of-sight in their WISE-2MASS-PS1 photo-z data. Top panel of Fig. 2 shows a  $60^\circ \times 60^\circ$  size patch of the galaxy catalogue, centered on the CS direction. At the center of the CS, there is an approximately 20% underdensity in galaxy counts, extending for a radius over  $20^\circ$ . We observed that the deepest part of this underdensity is slightly off-center with respect to the center of the Cold Spot estimated based on CMB data, but we only use this nominal center in our analysis to minimize posteriori choices.

The image in the WISE-2MASS galaxy catalogue is

compared to the same angular patch of the WMAP 9-year Internal Linear Combination (ILC) map (Bennett et al. 2013) and of the PLANCK SMICA map (Ade et al. 2013) in Fig. 2. An average  $70 \mu\text{K}$  temperature decrement of approximately 10 degree in size is clearly visible, corresponding to the CMB Cold Spot (Cruz et al. 2005).

### 2.2.2 Further large voids in WISE-2MASS?

We proceed with identifying underdensities in WISE-2MASS that are comparable to that of the CMB Cold Spot region. The galaxy density field was smoothed with a  $\sigma = 20^\circ$  Gaussian kernel to filter out all underdensities smaller than the angular radius of the supervoid found at the CS. All pixels as “cold” as the CS supervoid region have been selected. Our findings are summarized in Fig. 3. There is another large underdensity in the WISE-2MASS catalog that has similar angular size to the CS. Moreover, this underdensity is somewhat deeper in its center, as shown in Fig. 8. We deem the center of the void as the coldest pixel’s location at  $\ell \approx 101^\circ$ ,  $b \approx 46^\circ$ , and for simplicity we call it the Draco Supervoid to distinguish it from the CS void. The  $60^\circ \times 60^\circ$  size patch of the galaxy and the CMB field corresponding to the Draco Supervoid is shown in Fig. 4.

A 5-degree Gaussian smoothed version of the CS and the Draco void field is shown in Fig. 5.

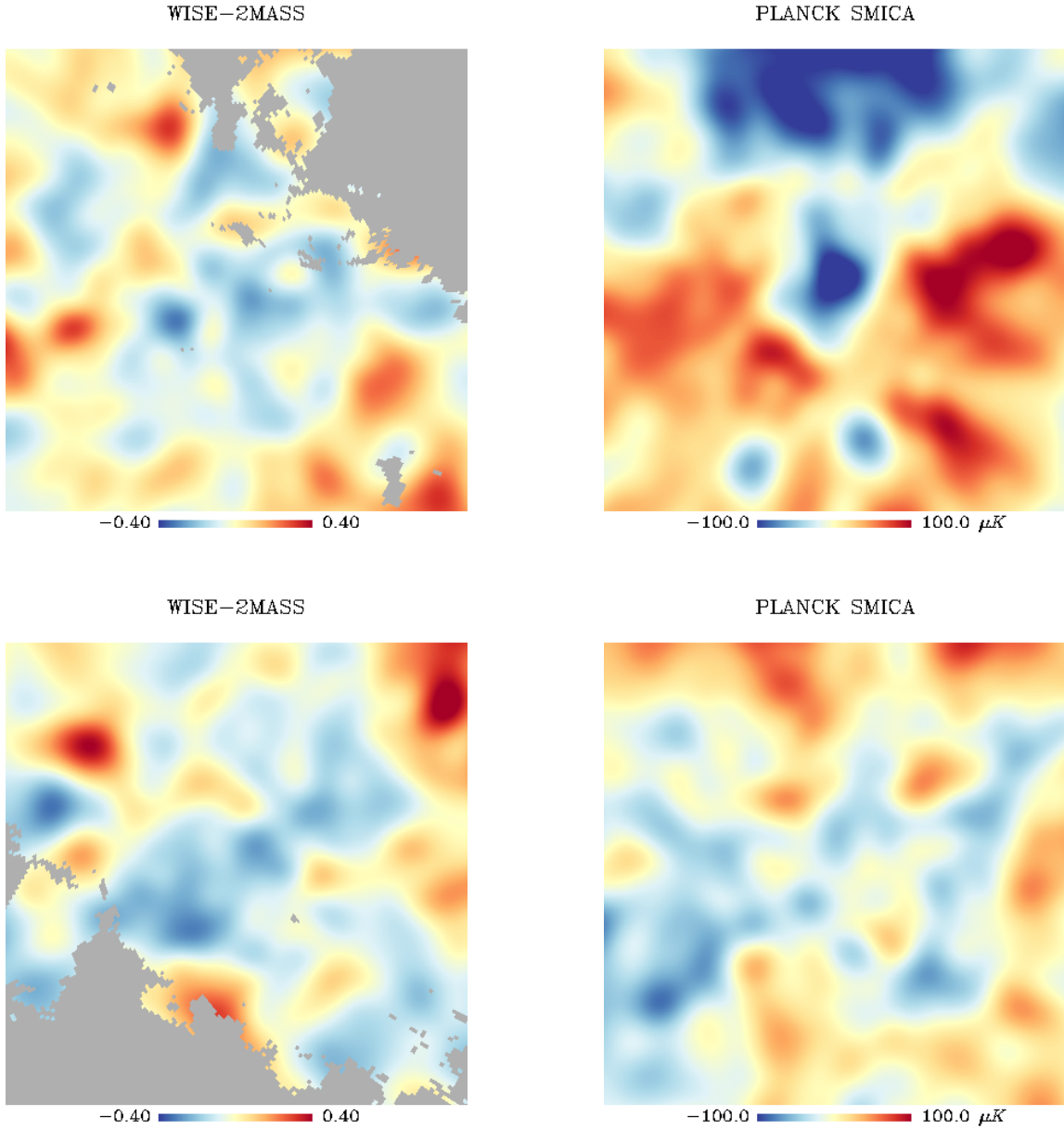


**Figure 5.** Top panels: The  $5^\circ$  Gaussian smoothed WISE-2MASS (left), and PLANCK SMICA (right) field in the direction of the Cold Spot. Bottom panels: same data in the direction of the Draco supervoid. The grey area in the WISE-2MASS panels shows the Galactic region we mask out for our analysis.

### 3 THE BASIC ALTB VOID MODEL

We model an underdensity in WISE-2MASS as a compensated void profile within a ALTB model, (García-Bellido and Haugboelle 2008),

$$ds^2 = -dt^2 + \frac{A'(r,t)^2}{1-k(r)} dr^2 + A(r,t)^2 d\Omega^2, \quad (1)$$

characterized by a spatial curvature profile given by

$$k(r) = k_0 r^2 \exp\left[-\frac{r^2}{r_0^2}\right]. \quad (2)$$

See also Romano et al. (2014) for a recent use of a Gaussian profile for LTB models in another context. We approx-

imate the novel ALTB model introduced above as a linear perturbation  $\Phi$  in the synchronous gauge in a Friedman-Robertson-Walker (FRW) metric with  $\Omega_M + \Omega_\Lambda = 1$ :

$$\Phi(\tau, r) = \Phi_0(r) \cdot {}_2F_1\left[1, \frac{1}{3}, \frac{11}{6}, -\frac{\Omega_\Lambda}{\Omega_M} a^3\right], \quad (3)$$

$$\equiv \Phi_0 \exp\left[-\frac{r^2}{r_0^2}\right] \cdot F_1(u) \quad (4)$$

where  $u = \frac{\Omega_\Lambda}{\Omega_M} a^3$  and  $\tau$  is the FRW conformal time:

$$\tau(a) = \frac{2\sqrt{a}}{H_0\sqrt{\Omega_M}} \cdot {}_2F_1\left[\frac{1}{2}, \frac{1}{6}, \frac{7}{6}, -\frac{\Omega_\Lambda}{\Omega_M} a^3\right] \equiv \frac{2\sqrt{a}}{H_0\sqrt{\Omega_M}} \cdot F_2(u). \quad (5)$$

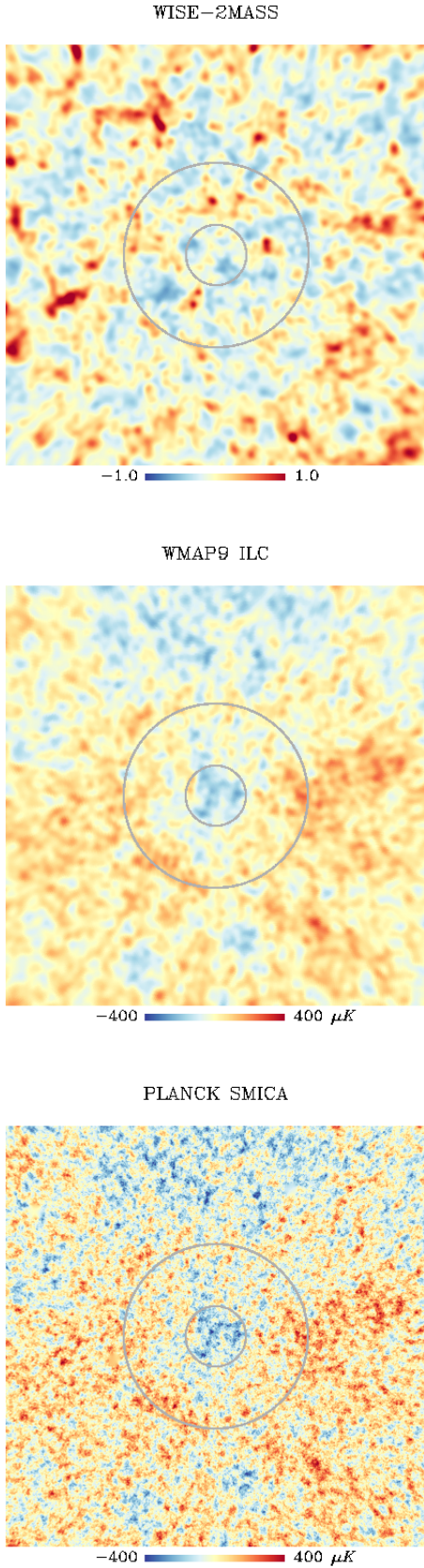


**Figure 2.** The WISE-2MASS (top), WMAP9 (middle), and PLANCK SMICA (bottom) field in the direction of the Cold Spot. Circles correspond to  $5^\circ$  and  $15^\circ$  radii.

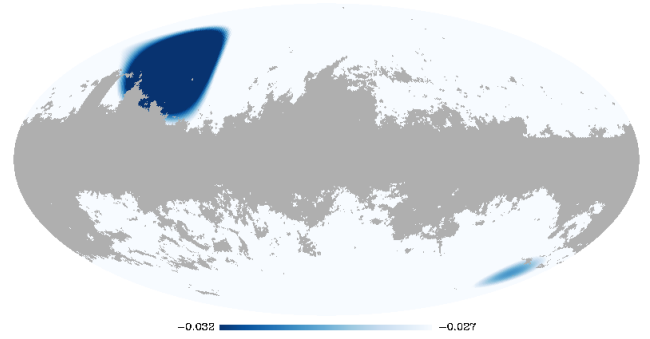


**Figure 3.** Applying a  $\sigma = 20^\circ$  Gaussian smoothing to the WISE-2MASS galaxy map one finds two large underdensities on the full observable sky. One of them is the famous Cold Spot region, the other one is the Draco supervoid.

The scalar potential (4) gives rise to a 3D density profile for the void, via Poisson equation  $\nabla^2 \Phi = \frac{3}{2} H_0^2 \Omega_M \delta / a$ ,

$$\delta(\tau, r) = -\delta_0 g(\tau) \left(1 - \frac{2}{3} \frac{r^2}{r_0^2}\right) \exp\left[-\frac{r^2}{r_0^2}\right], \quad (6)$$

characterized by two parameters, the comoving width of the void,  $r_0^2$ , and its depth today,  $\delta_0$ . The following relation between  $\Phi_0$ ,  $k_0$  and  $r_0$  holds:

$$\Phi_0 = \frac{-3k_0 r_0^2}{40} = \frac{\Omega_M}{4} \frac{H_0^2 r_0^2 \delta_0}{F_1(-\Omega_\Lambda/\Omega_M)}. \quad (7)$$

We write the density contrast growth factor  $g(a)$  as:

$$g(a) \equiv \frac{\delta(a)}{\delta(1)} = \frac{a \cdot F_1(u)}{F_1(-\Omega_\Lambda/\Omega_M)}.$$

It is easy to check that the 3D density profile (6) gives rise to a *compensated void*,

$$\int_0^\infty dr r^2 \delta(r, \tau) = 0, \quad (8)$$

a property which will be useful later.

In order to compare with WISE-2MASS, we project the 3D density (6) onto the transverse plane, with the center of the void at comoving distance  $y_0$ , see Fig. 6. The relation between  $r$  and  $\theta$  is given by  $r^2(y, \theta) = y^2 + y_0^2 - 2yy_0 \cos \theta$ ,

$$\delta_{2D}(\theta) = \int_0^\infty \delta(r(y, \theta)) y^2 \phi(y) dy, \quad (9)$$

with  $y = r(z)$  and  $y_0 = r(z_0)$  are the comoving distances to the void, and  $\phi(y)$  is the WISE-2MASS window function.

From the metric perturbation (4), we now compute the linear Integrated Sachs-Wolfe (ISW henceforth) (Sachs and Wolfe 1967; Kofman and Starobinsky 1985) and the non-linear Rees-Sciama (RS henceforth) (Rees and Sciama 1968)

<sup>2</sup> In a first version of this manuscript we followed Masina and Notari (2009) and considered a large difference between the FRW and the ALTB radii. This difference was due to an incorrect matching of the ALTB void to an Einstein-de Sitter model with  $\Omega_M = 1$ , which was performed by Biswas and Notari (2007) for a different physical problem. The FRW and  $\Lambda$ CDM radii are now approximately the same as in Zibin (2014); Nadathur et al. (2014).

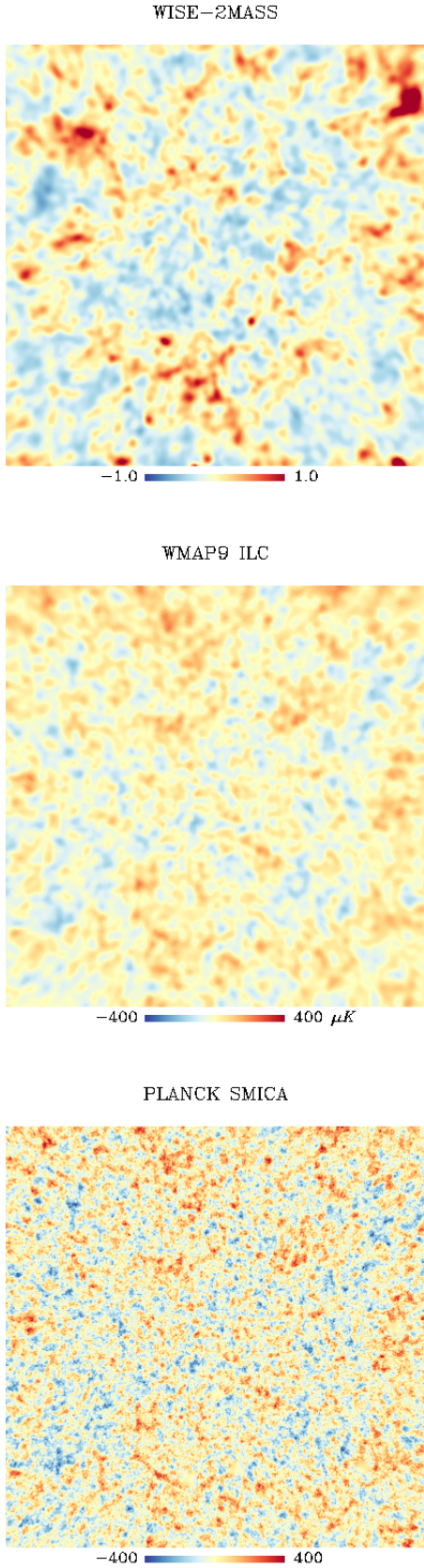


**Figure 4.** The WISE-2MASS (top), WMAP9 (middle), and PLANCK SMICA (bottom) field in the direction of the Draco void.

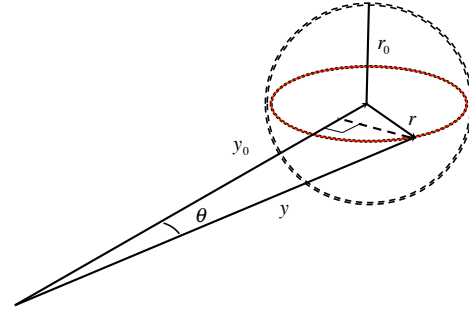


**Figure 6.** The corresponding geometry of the 2D projection of the LTB void for the WISE-2MASS projected galaxy contrast. The observer is at a comoving distance  $y_0$  from the center of the void.

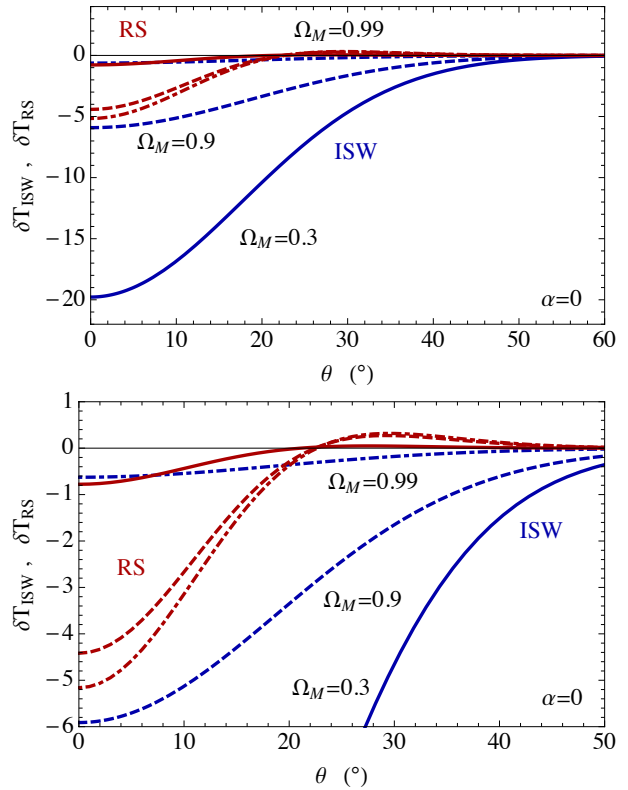


**Figure 7.** In the top panel the ISW (blue) and RS (red) effect for LTB voids with the profile introduced in Eq. (2) within our perturbative treatment are displayed for different values of  $\Omega_M = 0.3$  (solid),  $\Omega_M = 0.9$  (dashed),  $\Omega_M = 0.99$  (dot-dashed). In the bottom panel we zoom on the RS effect to show how its angular dependence differs from the one of the ISW term. The parameters of the void are  $r_0 = 195$  Mpc/h,  $\delta_0 = 0.25$ ,  $z_0 = 0.155$ .

effect on the CMB temperature anisotropies. For a large compensated void with a profile as in Eq. (6), the linear

ISW effect is given by

$$\begin{aligned} \frac{\delta T}{T}^{\text{ISW}}(\theta) &= 2 \int_{\tau_0}^{\tau_E} d\tau \dot{\Phi}(\tau, r) \\ &= -\frac{12}{11} \frac{\Omega_\Lambda}{\Omega_M} \int_0^1 da a^2 \Phi_0(r) \cdot {}_2F_1\left[2, \frac{4}{3}, \frac{17}{6}, \frac{-\Omega_\Lambda a^3}{\Omega_M}\right] \\ &\equiv -\frac{12}{11} \frac{\Omega_\Lambda}{\Omega_M} \int_0^1 da a^2 \Phi_0(r(z, \theta)) \cdot F_4(u), \end{aligned} \quad (10)$$

where

$$r^2(z, \theta) = r^2(z) + r^2(z_0) - 2r(z)r(z_0)\cos\theta,$$

and we integrate over  $z$ . Note that the comoving distance is given by  $r(z) = \tau_0 - \tau(z)$ , see Eq. (5).

For the Gaussian profile in Eq. (4) we find, in the small angle approximation, with  $r(z_0) > r_0$ ,

$$\begin{aligned} \frac{\delta T}{T}^{\text{ISW}}(\theta) &\simeq -\frac{3\sqrt{\pi}}{22} \frac{H(z_0)\Omega_\Lambda F_4(-\Omega_\Lambda/\Omega_M(1+z_0)^3)}{H_0(1+z_0)^4 F_1(-\Omega_\Lambda/\Omega_M)} \times \\ &\left(1 + \text{erf}\left[\frac{z_0}{H(z_0)r_0}\right]\right) \delta_0 (H_0 r_0)^3 \exp\left[-\frac{r^2(z_0)\theta^2}{r_0^2}\right], \end{aligned} \quad (11)$$

which also gives a Gaussian profile for the ISW effect.

Following Tomita (2005); Tomita and Inoue (2008), we compute the RS effect on the CMB temperature anisotropies as

$$\begin{aligned} \frac{\delta T}{T}^{\text{RS}}(\theta) &= \int_0^{z_{\text{LS}}} dz \left[ 4\zeta'_1(z) \frac{r^2(z, \theta)}{r_0^2} + 9\zeta'_2(z) \right] \times \\ &\frac{100}{9} \frac{\Phi_0^2}{r_0^2} \exp\left[-2\frac{r^2(z, \theta)}{r_0^2}\right], \end{aligned} \quad (12)$$

where primes denote differentiation w.r.t. redshift and

$$\zeta_1(z) = \frac{3\tau^2}{200} \cdot \frac{F_1^2(u)}{F_2^2(u)}, \quad (13)$$

$$\begin{aligned} \zeta_2(z) &= \frac{-\tau^2}{210} \cdot \frac{1}{F_2^2(u)} \left[ \frac{7}{5} \left( \frac{5}{6} F_1(u) + \frac{1}{6} F_3^2(u) \right) \right. \\ &\quad \left. - \frac{2}{5} \sqrt{1+u} \left( F_1(u) F_3(u) - \frac{5}{12} G(u) \right) \right], \end{aligned} \quad (14)$$

$$G(u) = \frac{1}{3} u^{-7/6} \int \frac{du u^{1/6}}{\sqrt{1+u}} [F_3^2(u) - F_1(u)]. \quad (15)$$

Doing the integral in  $z$ , in the small angle approximation,

$$\begin{aligned} \frac{\delta T}{T}^{\text{RS}}(\theta) &\simeq -\frac{100}{9} \sqrt{\frac{\pi}{8}} \left( 4\zeta'_1(z_0) \frac{r^2(z_0)}{r_0^2} \theta^2 + 9\zeta'_2(z_0) \right) H_0^2 \times \\ &\left( 1 + \text{erf}\left[\frac{\sqrt{2}z_0}{H(z_0)r_0}\right] \right) \frac{\Phi_0^2(r_0, \delta_0)}{H_0 r_0} \exp\left[-2\frac{r^2(z_0)}{r_0^2} \theta^2\right]. \end{aligned} \quad (16)$$

The ISW and RS effects are shown in Fig. 7. The RS effect is quadratic in  $\delta_0$  and cubic in  $r_0$ , but smaller than the ISW effect in a  $\Lambda$ CDM cosmology.<sup>3</sup>

### 3.1 Predictions for the Draco Supervoid

We construct a  $\chi^2$  statistics corresponding to the fits for the projected LTB model in the WISE-2MASS catalogue

<sup>3</sup> In a first version of this manuscript we evaluate a much larger RS effect, mainly due to a wrong mismatch between the LTB and FRW radius, following Masina and Notari (2009). Our RS (and ISW) calculation for the novel profile in Eq. (2) now agrees with Zibin (2014); Nadathur et al. (2014).

(denoted by the pedix LSS) and the corresponding effect on the PLANCK temperature anisotropy pattern (denoted by the pedix CMB). As primary parameters, we chose  $\{\theta_i\} = \{\delta_0, r_0, z_0\}$ , giving the following:

$$\chi_{\text{LSS}}^2 = \sum_{ij} (\delta_{2D}(\theta_i) - \delta_i^{\text{LSS}}) D_{ij}^{-1} (\delta_{2D}(\theta_j) - \delta_j^{\text{LSS}}), \quad (17)$$

$$\chi_{\text{CMB}}^2 = \sum_{ij} (\delta T(\theta_i) - \delta T_i^{\text{CMB}}) C_{ij}^{-1} (\delta T(\theta_j) - \delta T_j^{\text{CMB}}). \quad (18)$$

The term in Eq. (17) corresponds to the  $\chi^2$  of the projected LTB void profile (9) with respect to the observed WISE-2MASS galaxy distribution, using the highly correlated covariance matrix  $D_{ij}$  of concentric rings in WISE-2MASS. We estimated the covariances by generating 10,000 Gaussian realizations of the projected WISE-2MASS map with `Healpix synfast`. The simulations were created assuming PLANCK cosmology, and the redshift distribution of the WISE-2MASS sources.

The term in Eq. (18) is the  $\chi^2$  of the CMB profile compared to the covariance matrix of rings in the CMB is also highly correlated. The covariance matrix was determined from 10,000 Gaussian CMB realizations. Note the covariance of the CMB at the angular scales considered is dominated by cosmic variance, thus neglecting the cross-correlation with LSS is a good approximation.

In order to match the data to the LTB prediction, we followed Kovács et al. (2013) and Szapudi et al. (2015), and estimated the bias of the galaxy catalog using `SpICE` (Szapudi et al. 2001) and `python CosmoPy`<sup>4</sup> package, finding  $b = 1.41 \pm 0.07$ . The depression in galaxy counts, therefore, corresponds to a  $\delta_{2D} = \delta_{2D,g}/b$  underdensity in matter, assuming linear bias relation.

According to Eq. (17), the best-fit marginalized parameters to WISE-2MASS data alone is  $\delta_0 = 0.40 \pm 0.20$ ,  $r_0 = 210 \pm 70$  Mpc/h at 68 % CL. While from Eq. (18), the best-fit to PLANCK data alone is  $\delta_0 = 0.23 \pm 0.40$ ,  $r_0 = 290 \pm 90$  Mpc/h at 68 % CL<sup>5</sup>.

We now estimate a simultaneous fit of WISE-2MASS and PLANCK data by:

$$\chi_{\text{tot}}^2(\delta_0, r_0, z_0) = \chi_{\text{LSS}}^2 + \chi_{\text{CMB}}^2. \quad (19)$$

Simultaneous minimization yields the best fit parameters, which we quote here with marginalized  $1\sigma$  errors,

$$\delta_0 = 0.37_{-0.12}^{+0.22} (1\sigma), \quad (20)$$

$$r_0(\text{Mpc}/h) = 190_{-27}^{+39} (1\sigma), \quad (21)$$

$$z_0 = 0.15_{-0.05}^{+0.04} (1\sigma), \quad (22)$$

which are in good agreement with the best-fits obtained separately from WISE-2MASS and Planck, and with the WISE-2MASS window function. The  $1$  and  $2\sigma$  contours of the size and depth parameters of the LTB void are shown in Fig. 9.

Note that the only constraint on the redshift of the void center relies on the matching with the CMB profile in the

<sup>4</sup> <http://www.ifa.hawaii.edu/cosmopy/>

<sup>5</sup> The  $\chi^2$  statistic for the radial density profile measurement compared to a null value in each bin, and found  $\chi^2 = 65.22$  for 24 degrees-of-freedom, i.e.  $p = 10^{-5}$  as a simple estimate of the extremeness of the Draco supervoid in WISE-2MASS.

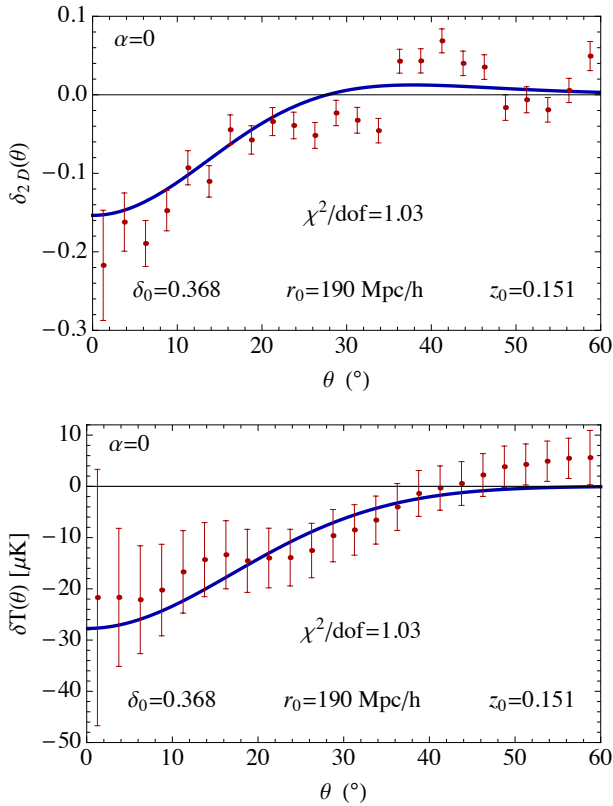


**Figure 8.** The density profile from WISE-2MASS catalogue compared with the best-fit theoretical model for the underdensity (9) from a combined analysis (top panel). The temperature profile from PLANCK SMICA map (bottom panel) is compared with the predicted CMB signal. The blue lines are the theoretical profiles for rings and in red are the measurements.

location of the supervoid, and assuming a particular LTB void model. The approximate central redshift of  $0.10 < z < 0.20$  is just compatible with our prior knowledge that the void might be located relatively close to us (Rassat et al. 2013). This slight tension indicates that in reality the void might be smaller in physical size and its cooling effect on the CMB is less significant assuming the same LTB model.

For later comparison, we calculate the averaged underdensity within the best fit radius  $r_0 = 190 h^{-1} \text{Mpc}$ . The 3D top-hat-averaged density from the LTB profile, see Eq. (6), is  $\bar{\delta} = 3/r_0^3 \int_0^{r_0} r^2 dr \delta(r) = -\delta_0/e$ . This finally gives the average void depth  $\bar{\delta} = -0.14 \pm 0.03$ .

In the  $\Lambda\text{CDM}$  model, the expected number of supervoids as extreme as the Draco supervoid at  $z < 0.5$  is roughly  $N \sim 10$  according to the estimations of Nadathur et al. (2014) in their Figure 5. However, for a more realistic modelling of the actual survey volume filled by the WISE-2MASS catalog, we need to take into account a masking factor  $f_{sky} = 0.53$ , and the fact that the redshift distribution of the WISE-2MASS catalog prevents reliable void identification at  $z \geq 0.25$ . The latter effectively results in a WISE-2MASS comoving survey volume that is only  $\sim 15\%$  of the volume considered in Nadathur et al. (2014). Including these factors, we estimate a probability of  $p \approx 0.8$  for finding a void at least as extreme as the Draco void in the WISE-2MASS survey volume.

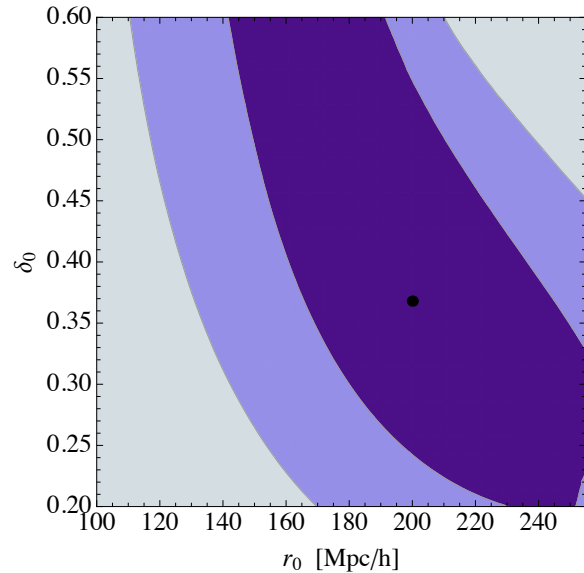


**Figure 9.** The 1 and  $2\sigma$  contours of the size and depth parameters of the LTB void (6), after marginalization over the redshift of the center of the void with the WISE-2MASS window function.

### 3.2 Modelling of the Cold Spot

We now analyze a LTB description for the supervoid found in the CS direction. By using the results in section IV we obtain the marginalized over redshift best-fit to WISE-2MASS data with reduced  $\chi^2 = 0.85$  and  $\delta_0 = 0.29 \pm 0.19$ ,  $r_0(\text{Mpc}/h) = 198 \pm 90$  at 68 % CL<sup>6</sup>. As best-fit to PLANCK data we obtain a reduced  $\chi^2 = 1.2$  and  $r_0(\text{Mpc}/h) = 136 \pm 50$ , at 68 % CL, with no constraint on  $\delta_0$ .

As is clear from the discussion above, the angular profile of the temperature decrement in the CS cannot be properly fit by the ISW+RS effect described in Section III. The CMB imprint computed in Section 3 does not exhibit any ridge about 15 degrees which instead characterizes the CS (Zhang and Huterer (2010) noticed this structure as an outer ring).

We therefore modify the basic LTB profile by introducing a new parameter  $\alpha$ ,

$$\Phi_0(r) = \Phi_0 \left(1 - \alpha \frac{r^2}{r_0^2}\right) \exp\left[-\frac{r^2}{r_0^2}\right] \quad (23)$$

which corresponds to a density contrast:

$$\delta(\tau, r) = -\delta_0 g(\tau) \left(1 - \frac{2 + 7\alpha}{3 + 3\alpha} \frac{r^2}{r_0^2} + \frac{2\alpha}{3 + 3\alpha} \frac{r^4}{r_0^4}\right) e^{-r^2/r_0^2}, \quad (24)$$

again giving rise to a *compensated void* (8), for all  $\alpha$ . With these modifications, the ISW and RS angular profiles, for

<sup>6</sup> The  $\chi^2$  statistic for the radial density profile measurement compared to the null value in each bin is 43.94 for 24 degrees-of-freedom, i.e.  $p = 0.007$ .



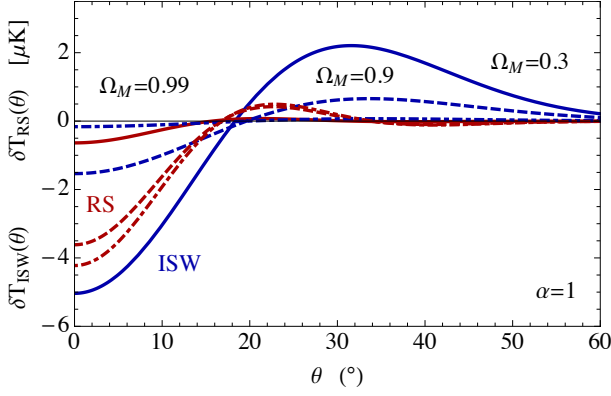


**Figure 10.** In the top panel the ISW (blue) and RS (red) effect for LTB voids with the profile introduced in Eq. (23) within our perturbative treatment are displayed for different values of  $\Omega_M = 0.3$  (solid),  $\Omega_M = 0.9$  (dashed),  $\Omega_M = 0.99$  (dot-dashed). Note how for  $\alpha = 1$  the angular profiles of the ISW and RS effects still differ, but now the ISW term exhibits a profile similar to a compensated one. The parameters of the void are  $r_0 = 195$  Mpc/h,  $\delta_0 = 0.25$ ,  $z_0 = 0.155$ .

$0 < \alpha < 2$ , are given by

$$\frac{\delta T^{\text{ISW}}}{T}(\theta) \simeq -\frac{3\sqrt{\pi}}{22} \frac{H(z_0)\Omega_\Lambda \cdot F_4(-\Omega_\Lambda/\Omega_M(1+z_0)^3)}{(1+\alpha)H_0(1+z_0)^4 \cdot F_1(-\Omega_\Lambda/\Omega_M)} \times \left(\frac{2-\alpha}{2} - \alpha \frac{r^2(z_0)}{r_0^2} \theta^2\right) \left(1 + \text{erf}\left[\frac{z_0}{H(z_0)r_0}\right]\right) \times \delta_0 (H_0 r_0)^3 \exp\left[-\frac{r^2(z_0)}{r_0^2} \theta^2\right], \quad (25)$$

which now has a node and a positive maximum, and

$$\frac{\delta T^{\text{RS}}}{T}(\theta) \simeq -\frac{100}{9} \sqrt{\frac{\pi}{8}} \left[9\zeta'_2(z_0) \left(1 + \frac{\alpha}{2} + \frac{7}{16}\alpha^2\right) + \left(4\zeta'_1(z_0) \left(1 + \frac{\alpha}{2}\right) - 9\zeta'_2(z_0) \left(2\alpha + \frac{\alpha^2}{2}\right)\right) \frac{r^2(z_0)}{r_0^2} \theta^2 + \left(9\zeta'_2(z_0)\alpha^2 - 4\zeta'_1(z_0)\alpha\right) \frac{r^4(z_0)}{r_0^4} \theta^4\right] H_0^2 \times \left(1 + \text{erf}\left[\frac{\sqrt{2}z_0}{H(z_0)r_0}\right]\right) \frac{\Phi_0^2(r_0, \delta_0)}{H_0 r_0} \exp\left[-2\frac{r^2(z_0)}{r_0^2} \theta^2\right]. \quad (26)$$

These two effects are shown in Fig. 10. Note how this new compensated void model leads to a completely different angular profile for the ISW term, reminiscent of a compensated structure in the CMB as well, although with a smaller amplitude with respect to  $\alpha = 0$ .

We choose from now on the parameter  $\alpha = 1$ . We then obtain a best-fit to WISE-2MASS data with reduced  $\chi^2 = 0.85$  (for 24 d.o.f.) and  $\delta_0 = 0.27 \pm 0.25$ ,  $r_0$ (Mpc/h) =  $270 \pm 90$  at 68 % CL. By fitting to PLANCK data alone we obtain a similar radius,  $r_0$ (Mpc/h) =  $254 \pm 50$  at 68 % CL, with a large underdensity,  $\delta_0 > 0.6$  at 95 % CL, which is clearly too high for the  $\Lambda$ CDM model.

Our ALTB models for the WISE-2MASS underdensity and the CMB decrement in the direction of the CS are not as satisfactory as for the analogous alignment we have found in the direction of the Draco Supervoid. Although we have introduced a second novel compensated LTB profile, which leads to an ISW plus RS angular profile reminiscent of the CMB decrement in the direction of the CS, we cannot find

an amplitude which fits well WISE-2MASS and PLANCK simultaneously for  $\alpha = 1$ .

Given the current status of the WISE-2MASS observations, we cannot exclude that other values of  $\alpha$  or other profiles could provide a better fit. Another issues are the approximations used in this paper, as the perturbative treatment in a flat FRW metric, the assumption of  $\Lambda$ CDM, or spherical symmetry. It is conceivable that the structure in the direction of the CS might not be well approximated by a spherical object and might be possibly elongated along the line of sight: in such a case the angular profile in the WISE-2MASS data would be smaller than the effective distance which enters in the CMB decrement. Although this calculation goes beyond the scope of the current paper, this different geometry for the underdensity would help in reconciling the amplitude of the CMB decrement with the underdensity seen in WISE-2MASS.

In fact, if we consider together two adjacent voids along the same line of sight, at two different redshifts, it is possible to find a reasonable minimum  $\chi^2$ , at the expense of an unrealistic depth (i.e. high density contrast) for the furthest void, although with reasonable widths in both, see Fig. 11. The common reduced  $\chi^2 = 0.96$  for the first void at  $z_0 = 0.2$  with a width  $r_0 = 220$  Mpc/h and depth  $\delta_0 = 0.25$ , and for the second void at  $z_0 = 0.5$  with a width  $r_0 = 350$  Mpc/h and depth  $\delta_0 = 0.5$  with reduced  $\chi^2 = 17.4/24$  d.o.f. for WISE-2MASS and  $\chi^2 = 12.5/10$  d.o.f. for PLANCK.

For estimations of the cosmic rareness of the CS void, we rely on the (presumably more accurate) best-fit void parameters obtained with photo-z mapping by the companion paper Szapudi et al. (2015) ( $\delta_{2D} = 0.14$ ,  $\delta_0 = 0.38$ ,  $r_0 = 220$  Mpc/h). The probability of detecting supervoids at least as extreme as the CS supervoid at  $z < 0.5$  is roughly  $p \sim 0.1$  according to the estimations of Nadathur et al. (2014). Including the  $f_{sky} = 0.53$  and  $V_{z < 0.25}/V_{z < 0.5} \approx 0.15$  factors, the estimated probability is  $p \sim 0.01$  for finding a void at least as extreme as the CS void in the WISE-2MASS survey volume. Thus the CS void represents a rare fluctuation in  $\Lambda$ CDM, and its occurrence is less likely than that of the Draco Supervoid. Note that the large errors on  $\delta_0$  and  $r_0$  can result in drastic changes in the expected void probability and ISW-RS signal of such voids (Nadathur et al. 2014). We, therefore, refer to these probabilities as crude estimations of cosmic rareness.

## 4 DISCUSSION & CONCLUSIONS

We have found two large underdensities in the WISE-2MASS catalogue (Kovács and Szapudi 2014) smoothed on  $20^\circ$  scales. The Draco supervoid is located at  $(l, b) \approx (101^\circ, 46^\circ)$  and it corresponds to a gentle decrement in the CMB observed by both WMAP and PLANCK, and it is well explained by the ISW and RS effects. The other supervoid is in the well known direction of the CMB CS, and its explanation in terms of ISW and RS effect is less satisfactory. Nevertheless, observationally, we found that the two most prominent supervoids identified in a full sky catalog coincide with cold areas of the CMB.

A related project Szapudi et al. (2015) used the same WISE-2MASS data set supplemented with PS1 photometric redshifts and the data by Granett, Szapudi and Neyrinck

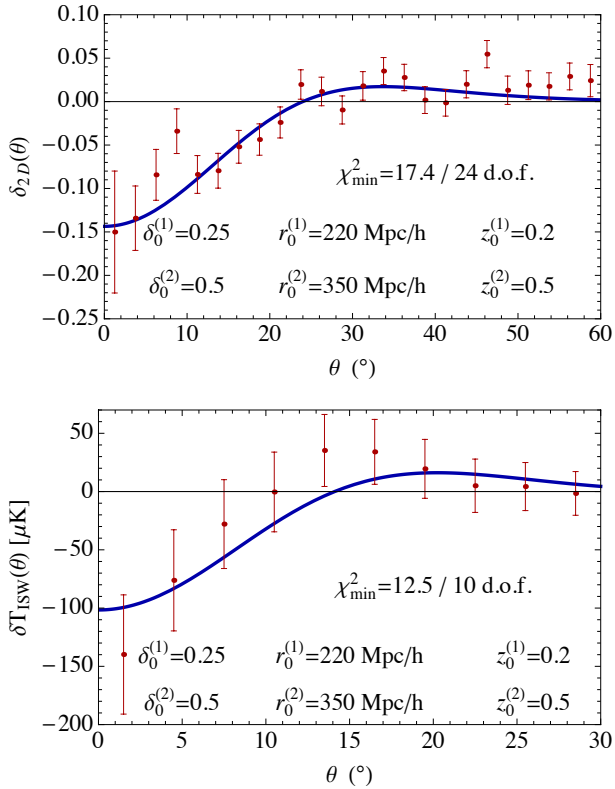


**Figure 11.** The density profile from WISE-2MASS catalogue compared with the theoretical model for the underdensity (9) (top panel). The temperature profile from PLANCK SMICA map (bottom panel) is compared with the predicted CMB signal. The blue lines are the theoretical profiles for rings and in red are the measurements. The model considers two adjacent spherical voids along the same line of sight with different sizes and depths.

(2010b) for a direct tomographic imaging of the CS region. They found a supervoid at  $z = 0.22 \pm 0.03$  with radius  $r_0 = 220 \pm 50 h^{-1} \text{Mpc}$  and depth of  $\delta = -0.14 \pm 0.04$ .

Motivated by these findings, we developed novel spherically symmetric ALTB compensated void models to explain the CMB decrements observed in the direction of the two largest underdensities (supervoids) of the WISE-2MASS catalogue. We compute perturbatively the projected angular density profile, and the ISW and RS angular profiles following the second order treatment presented in Tomita (2005); Tomita and Inoue (2008).

Within our perturbative treatment of the simplest family of LTB voids introduced here with a Gaussian profile for the curvature, we find that the Integrated Sachs-Wolfe and Riess-Sciama effects due to the Draco Supervoid found in the WISE-2MASS catalogue can explain well the CMB decrement observed in the same direction. By considering the combined fit with WISE-2MASS catalogue and PLANCK we obtain  $\delta_0 = 0.37^{+0.22}_{-0.12}$ ,  $r_0(\text{Mpc}/h) = 190^{+39}_{-27}$ ,  $z_0 = 0.15^{+0.04}_{-0.05}$  at  $1\sigma$  as a best-fit. The estimated redshift of the underdensity is in good agreement with the WISE-2MASS window function, but 2MASS-only observations of this underdense region by Rassat et al. (2013) indicate that the Draco void might be located closer to us, and therefore slightly smaller in physical size.

The explanation of the large decrement for the CS in

terms of the ISW and RS effects is known to be difficult (Inoue and Silk 2006, 2007). The CMB angular profile of the CS, studied here at larger angular distances than those commonly considered ( $\sim 10^\circ$ ), constitute also a puzzle with respect to the standard angular profiles previously studied (Inoue and Silk 2006, 2007) and those obtained here with the perturbative treatment of the simplest class of LTB voids. By introducing a further generalization of the LTB voids, which allows a more radical compensation, we indeed find an angular profile which better mimics what is observed in the CS, but with a much smaller amplitude for the underdensity found in the redshift range of the WISE-2MASS catalogue.

Given the status of the LSS observations and the assumptions used in this paper, more precise observations and further theoretical developments are needed before the CMB CS will be satisfactorily explained. On the observational ground, the 21,200  $\text{deg}^2$  photometric redshift catalog of WISE-2MASS galaxies matched with SuperCOSMOS data (Kovács et al., in preparation) will provide an enhanced tool for examining these structures and for identifying more superstructures in the low- $z$  Universe.

Concerning the assumption of  $\Lambda\text{CDM}$ , there is some debate about the effects on the CMB being stronger than the simple predictions of the linear ISW model in a  $\Lambda\text{CDM}$  cosmology (e.g., Granett, Szapudi and Neyrinck 2008, 2010a; Papai and Szapudi 2010; Cai et al. 2014). We also mention how the assumption of spherical symmetry or the use of perturbation theory or the absence of cross-correlation between the SW and ISW terms in our calculation could be important quantitative aspects, which go beyond the scope of the present project.

Despite the assumptions and caveats mentioned above, let us finally note that this work, and the related project Szapudi et al. (2015), significantly increased the probability of a physical explanation of the CS instead of a statistical fluke. Given the rareness of the supervoid found in the CS direction, estimated here at about a  $3\sigma$  deviation, we could ask for the probability of a random alignment of such a supervoid in the WISE-2MASS with a rare fluctuation in the CMB as the Cold Spot. Even considering the CS only as a  $2\sigma$  fluctuation, the hypothesis of this alignment as a statistical fluke is quite low. We presented a quasi-linear ISW term with an angular profile similar to the CS and an amplitude larger than  $20 \mu\text{K}$  obtained within spherical symmetry. Thus a fairly typical cold primordial fluctuation enhancing the ISW effect from the CS void on the CMB sky could provide a plausible explanation.

## ACKNOWLEDGEMENTS

FF and JGB wish to thank the bilateral agreement INFN-CICYT and in particular the director of the Bologna INFN section Dr. G. Bruni for partially supporting this project. FF acknowledges the support by ASI through ASI/INAF Agreement I/072/09/0 for the PLANCK LFI Activity of Phase E2 and by MIUR through PRIN 2009 grant no. 2009XZ54H2. JGB acknowledges financial support from the Madrid Regional Government (CAM) under the program HEPHACOS S2009/ESP-1473-02, from the Spanish MICINN grants AYA2009-13936-C06-06, FPA2012-39684-C03-02 and Consolider-Ingenio 2010 PAU (CSD2007-00060),

and from the MINECO Centro de Excelencia Severo Ochoa Programme, grant SEV-2012-0249. In addition, AK takes immense pleasure in thanking the support provided by the Campus Hungary fellowship program. Funding for this project was partially provided by the Spanish Ministerio de Economía y Competitividad (MINECO) under projects FPA2012-39684, and Centro de Excelencia Severo Ochoa SEV-2012-0234. IS acknowledges support from NASA grants NNX12AF83G and NNX10AD53G.

## REFERENCES

- Abazajian K. N., Adelman-McCarthy J. K., Agüeros M. A., Allam S. S., Allende Prieto C., An D., Anderson K. S. J., Anderson S. F., Annis J., Bahcall N. A., et al. 2009, *Astrophys. J. Suppl.* **182**, 543
- LSST Science Collaboration Abell P. A., Allison J., Anderson S. F., Andrew J. R., Angel J. R. P., Armus L., Arnett D., Asztalos S. J., Axelrod T. S., et al. 2009, *ArXiv e-prints*
- Ade P. A. R. *et al.* [Planck Collaboration], 2013, “Planck 2013 results. I. Overview of products and scientific results,” *arXiv:1303.5062 [astro-ph.CO]*.
- Ade P. A. R. *et al.* [Planck Collaboration], 2013, *Astron. Astrophys.* **571** (2014) A12
- Ade P. A. R. *et al.* [Planck Collaboration], 2013, *Astron. Astrophys.* **571** (2014) A23
- P. A. R. Ade *et al.* [Planck Collaboration], *Astron. Astrophys.* **571** (2014) A19
- Afshordi N., Slosar A. and Wang Y., 2011, *JCAP* **1101** 019
- Amendola L. *et al.* [Euclid Collaboration], 2013, *Living Reviews in Relativity* **16**, 6
- Bennett C. L. *et al.* [WMAP Collaboration], 2013, *Astrophys. J. Suppl.* **208** 20
- Bennett C. L. *et al.* [WMAP Collaboration], 2003, *Astrophys. J. Suppl.* **148** 1
- Bremer M. N., Silk J., Davies L. J. M. and Lehnert M. D., 2010, *Mon. Not. Roy. Astron. Soc. Letters* **404** 69
- Y. C. Cai, M. C. Neyrinck, I. Szapudi, S. Cole and C. S. Frenk, *Astrophys. J.* **786** (2014) 110 [*arXiv:1301.6136 [astro-ph.CO]*].
- Cardoso J.-F., Martin M., Delabrouille J., Betoule M. and Patanchon G., 2008, *IEEE Journal of Selected Topics in Signal Processing* **2**, 735.
- Colberg J. M., Sheth R. K., Diaferio A., Gao L. and Yoshida N., 2005, *Mon. Not. Roy. Astron. Soc.* **360** 216
- Cruz M., Martinez-Gonzalez E., Vielva P. and Cayon L., 2005, *Mon. Not. Roy. Astron. Soc.* **356** 29
- Cruz M., Tucci M., Martinez-Gonzalez E. and Vielva P., 2006, *Mon. Not. Roy. Astron. Soc.* **369** 57
- Cruz M., Turok N., Vielva P., Martinez-Gonzalez E., and Hobson M., 2008, *Mon. Not. Roy. Astron. Soc.* **390** (2008) 913
- Cruz M., Martinez-Gonzalez E., Vielva P., Diego J. M., Hobson M. and Turok N., 2008, *Mon. Not. Roy. Astron. Soc.* **390** (2008) 913
- Das S. and Spergel D.N., *Phys. Rev. D* **79** (2009) 043007
- Driver S. P., Hill D. T., et al. 2011, *Mon. Not. Roy. Astron. Soc.* **413**, 971
- Francis C. L., Peacock J. A., 2010, *Mon. Not. Roy. Astron. Soc.* **406**, 2.
- Francis C. L., Peacock J. A., 2010, *Mon. Not. Roy. Astron. Soc.* **406**, 14
- García-Bellido J. and Haugboelle T., 2008, *JCAP* **0804** 003
- Gorski K. M., Hivon E., Banday A. J., Wandelt B. D., Hansen F. K., Reinecke M. and Bartelman M., *Astrophys. J.* **622** (2005) 759
- B. R. Granett, M. C. Neyrinck and I. Szapudi, *Astrophys. J.* **683** (2008) L99
- B. R. Granett, M. C. Neyrinck and I. Szapudi, *Astrophys. J.* **701** (2009) 414
- Granett B. R., Szapudi I. and Neyrinck M. C., 2010, *Astrophys. J.* **714** 825
- Inoue K. T. and Silk J., 2006, *Astrophys. J.* **648** 23
- Inoue K. T. and Silk J., 2007, *Astrophys. J.* **664** 650
- Inoue K. T., Sakai N. and Tomita K., 2010, *Astrophys. J.* **724**, 12
- Inoue K. T., 2012, *Mon. Not. Roy. Astron. Soc.* **421** 2731
- T. H. Jarrett, T. Chester, R. Cutri, S. Schneider, M. Skrutskie, J. P. Huchra, 2000, *Astrophys. J.* **119**, 2498
- Kaiser N., Burgett W., Chambers K., 2010, ‘Society of Photo-Optical Instrumentation Engineers (SPIE) Conference Series’, 773
- L. Kofman and A. A. Starobinsky, *Sov. Astron. Lett.* **11** (1985) 271 [*Pisma Astron. Zh.* **11** (1985) 643].
- Kovács A., Szapudi I., Granett B. R. and Frei Z., 2013, *MNRAS Letters* **431**, L 28.
- Kovács A. and Szapudi I., 2014, *arXiv:1401.0156*, submitted to *MNRAS*
- E. D. Kovetz and M. Kamionkowski, *Phys. Rev. Lett.* **110** (2013) 17, 171301
- Laureijs R. *et al.* [Euclid Collaboration], Euclid definition study report, [*arXiv:1110.3193 [astro-ph.CO]*].
- T. Biswas and A. Notari, *JCAP* **0806** (2008) 021
- Masina I. and Notari A., *JCAP* **0902** (2009) 019
- S. Nadathur, M. Lavinto, S. Hotchkiss and S. Rsnen, *Phys. Rev. D* **90** (2014) 10, 103510, [*arXiv:1408.4720 [astro-ph.CO]*].
- P. Papai and I. Szapudi, *Astrophys. J.* **725** (2010) 2078
- P. Papai, I. Szapudi and B. R. Granett, *Astrophys. J.* **732** (2011) 27
- Rassat, A. and Starck, J.-L. and Dupé, F.-X., *A&A* **557** (2013) A32
- Rees, M. J. & Sciama, D. W., *Nature* **217** (1968) 511
- A. Enea Romano, S. Sanes, M. Sasaki and A. A. Starobinsky, *Europhys. Lett.* **106** (2014) 69002
- Rudnick L., Brown S. and Williams L. R., 2007, *Astrophys. J.* **671**, 40.
- Sachs, R. K. & Wolfe, A. M., *Astrophys. J.* **147** (1967) 73
- Schlegel, D. J. and Finkbeiner, D. P. and Davis, M., 1998, *arXiv:9710327*.
- M. Levi *et al.* [DESI Collaboration], “The DESI Experiment, a whitepaper for Snowmass 2013,” *arXiv:1308.0847 [astro-ph.CO]*.
- Smith K. M and Huterer D., 2010, *Mon. Not. Roy. Astron. Soc.* **403** 2.
- Skrutskie M. F. et al., 2006, *Astron. J.* **131**, 1163
- Szapudi, I. and Prunet, S. and Pogosyan, D. and Szalay, A. S. and Bond, J. R., 2001, *arXiv:0010256*
- Szapudi, I. et al., 2015, *M.N.R.A.S.*, 450, 288
- K. Tomita, *Phys. Rev. D* **71** (2005), 083504
- K. Tomita and K. T. Inoue, *Phys. Rev. D* **77** (2008), 103522
- Vielva P., Martinez-Gonzalez E., Barreiro R. B., Sanz J. L.

- and Cayon L., 2004, *Astrophys. J.* **609** 22  
Vielva P., 2010, *Adv. Astron.* **2010** 592094.  
Vilenkin A. and Shellard E.P.S., “Cosmic Strings and other  
Topological Defects”, Cambridge U.P. (1994).  
Wright E. L. et al., 2010, *Astron. J* **140**, 1868  
Zhang R. and Huterer D., 2010, *Astropart. Phys.* **33**, 69  
J. P. Zibin, arXiv:1408.4442 [astro-ph.CO].